



Microfluidic elaboration of polymer microfibers from miscible phases: Effect of operating and material parameters on fiber diameter

Wasif Razzaq, Christophe A Serra, Leandro Jacomine, Delphine Chan-Seng

► To cite this version:

Wasif Razzaq, Christophe A Serra, Leandro Jacomine, Delphine Chan-Seng. Microfluidic elaboration of polymer microfibers from miscible phases: Effect of operating and material parameters on fiber diameter. Journal of the Taiwan Institute of Chemical Engineers, 2022, 132, pp.104215. 10.1016/j.jtice.2022.104215 . hal-03548832

HAL Id: hal-03548832

<https://hal.science/hal-03548832v1>

Submitted on 31 Jan 2022

HAL is a multi-disciplinary open access archive for the deposit and dissemination of scientific research documents, whether they are published or not. The documents may come from teaching and research institutions in France or abroad, or from public or private research centers.

L'archive ouverte pluridisciplinaire **HAL**, est destinée au dépôt et à la diffusion de documents scientifiques de niveau recherche, publiés ou non, émanant des établissements d'enseignement et de recherche français ou étrangers, des laboratoires publics ou privés.

Microfluidic Elaboration of Polymer Microfibers from Miscible Phases: Effect of Operating and Material Parameters on Fiber Diameter

Wasif Razzaq^{1,2}, Christophe A. Serra,^{1*} Leandro Jacomine¹, Delphine Chan-Seng¹

¹ Université de Strasbourg, CNRS, Institut Charles Sadron UPR 22, F-67000 Strasbourg, France

Email: ca.serra@unistra.fr, +33 3.88.41.40.95

² Department of Materials Engineering, National Textile University, Sheikhupura Road, Faisalabad, 37610, Pakistan

Keywords: microfluidics, microfiber diameter, photopolymerization, capillary number

Background: fiber diameter is one of the most important morphological parameters which drives the applications of microfibers. This creates a need for the development of processes capable of producing a large variety of microfibers with a given diameter. To this regards, microfluidic spinning has recently emerged as an outstanding and simple technique for the production of micro- and nanofibers with controllable size and morphology.

Methods: herein, microfibers were produced from (macro)monomers or prepolymers (core phase) by *in situ* photoirradiation using a capillary-based microfluidic device and a miscible sheath phase of various viscosity. The effects of the flow rate of both phases as well as the viscosity of the sheath fluid, the capillary dimensions and the monomer volume fraction in core phase were thoroughly studied.

Significant findings: by calculating the capillary number ratio from the ratios of sheath to core flow rate and viscosity, an empirical relationship which perfectly predicts the microfiber diameter as a function of monomer volume fraction, the capillary number ratio and capillary inner diameter but independent of its outer diameter is extracted. This result paves the way to the continuous-flow production of microfibers with well-controlled morphological characteristics.

1. Introduction

Microfibers have attracted a lot of attention due to i) their large surface area to volume ratio, ii) their diverse properties arising from the great variety of materials they are made of, and iii) their ability to assemble into 3D complex structures and foldability.[1] These benefits enable polymer microfibers to have an excellent potential in many applications such as biomedicine,[2-6] fiber optics,[7] sensors,[8, 9] and water treatment.[10, 11] Different approaches have been employed to produce micro- and nanofibers such as melt spinning,[12] wet spinning,[13] draw spinning,[14] macromolecular assembly,[15] and electrospinning,[16] techniques relying on the physical mechanism of solidification to produce fibers, *i.e.* the starting raw material is a polymer solution. As such they suffer from limitations regarding i) the nature of the material employed and ii) the morphologies of fibers that can be achieved.[17] Hence, it is difficult to produce fibers with diverse morphologies and with a broad range of materials. Recently, microfluidic spinning has shown a great potential for the production of microfibers with diverse compositions, morphologies, and surface functionalities. This technique consists in stretching a stream of monomer or polymer solution (core phase) by an immiscible or miscible solution (continuous or sheath phase) inside a microfluidic device. Due to the small size of the device microchannel (*ca.* 100 μm), laminar flow is commonly achieved affording reproducibility and stability to the flow; two highly desirable features required for the production of fibers with given diameters and morphologies. By manipulating the flow inertia (*i.e.* individual solution flow rates), solution viscosity, interfacial tension between the core and sheath phases and taking possibly advantage of gravity forces, fibers with diverse morphologies such as grooved, flat, core-shell, hollow, and Janus can be easily produced. The choice of material becomes broader due to the panel of solidification methods, *i.e.* photopolymerization, ionic and chemical crosslinking, solvent exchange, and solvent evaporation. Fiber surface functionalization is also possible by encapsulation method or *in situ* chemistry.[1] Surface to volume ratio is one of the foremost fiber parameters that drive their applications. Since the latter is inversely proportional to the fiber diameter,[18] many properties such as

mechanical,[19, 20] cell adhesion and proliferation,[20] biomimicking extracellular matrix,[21] optical extinction capacity,[22] and filtration performance[23] depend on the fiber diameter. Although, fiber diameter is a crucial parameter, the literature scarcely and partially reports on all the possible parameters responsible for controlling the fiber diameter in microfluidic spinning. Most reports address only the effect of sheath/continuous fluid and core/disperse fluids flow rates independently[24, 25] or in the form of sheath to core flow rate ratio (Q_s/Q_c) [26-29]. Liu *et al.* observed the effect of the capillary diameter on the fiber diameter using the thermoinitiated polymerization induced phase separation technique[30]. But there is no literature in which researchers interpreted these results into some mathematical form to predict the fiber diameters. Herein, we developed an empirical relationship which can predict the fiber diameter in relation with others operating and materials parameters for the case where the monomer and its polymer are miscible with the continuous phase. The investigation of operating parameters was not only limited to flow rates and capillary diameter, but the effect of viscosity of sheath fluid and monomer volume fraction in core phase was also investigated. Two monomers, tri(propylene glycol) diacrylate (TPGDA), poly(ethylene glycol) diacrylate (PEGDA), and one prepolymer, UV-curable adhesive NOA 89, were used as reference materials for the synthesis of fibers using *in situ* photoirradiation in a capillary-based microfluidic device. All results were used to extract an empirical correlation which predicted the final microfiber diameter upon variation of the capillary number ratio, monomer volume fraction, and internal capillary diameter.

2. Results and Discussion

The fibers were produced using a capillary-based microfluidic device (**Fig. 1**) involving two phases: 1) the core fluid (Φ_c) becoming the fiber upon photopolymerization and 2) the sheath fluid (Φ_s) consisting in poly(ethylene glycol) (PEG), whose flow rates are Q_c and Q_s respectively. PEG was used due to its miscibility with core fluid, commercial availability, high tunable

viscosity with its molecular weight which prevents fast diffusion of Φ_c into Φ_s , and reasonable shearing force to produce thinner fibers. Φ_c comprised a diacrylate (TPGDA, PEGDA, or NOA 89) in ethanol in the presence of Irgacure 369 as photoinitiator.

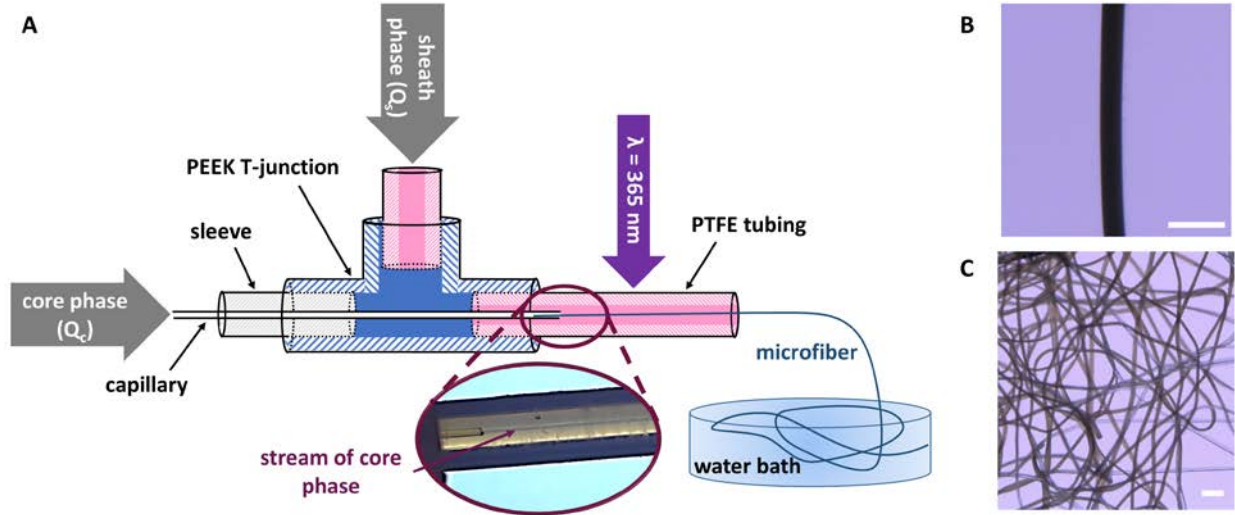


Fig. 1. (A) Capillary-based microfluidic device used to produce microfibers: Φ_s delivered from the top and Φ_c from the left of the T-junction using syringe pumps. The tip of the capillary, where Φ_s and Φ_c came into contact, has been magnified (inset). Numerical optical images of a single (B) and bundle (C) of fibers (scale bar = 100 μm).

2.1. Effect of the flow rate ratio Q_s/Q_c

The effect of sheath and core flow rates on the fiber diameter was investigated showing a decrease of the fiber diameter as the flow rate of Φ_s increased due to the increase in the shearing and stretching force exerted by Φ_s over Φ_c . On the other hand, the diameter increased with an increase in the flow rate of Φ_c , because of the widening of the jet due to the increase in the volume of Φ_c injected.[31-34] To observe the overall impact of the flow rate on the fiber diameter, the effect of Q_s/Q_c on the fiber diameter instead of individual flow rates was studied using PEG 300 as Φ_s . In a first set of experiments, Q_s was changed while keeping Q_c constant to have different values of Q_s/Q_c (110, 150, 190, 230 and 280). In another set of experiments, the core flow rate was changed while keeping the sheath flow rate constant to produce the same values of Q_s/Q_c . The values of

diameters produced in both set of experiments were similar (**Fig. 2**) meaning that the same Q_s/Q_c produced fibers of same diameters irrespective of the individual values of Q_s or Q_c . The reduction in diameter with the increase in Q_s/Q_c observed here has been also reported by other researchers.[35-37]

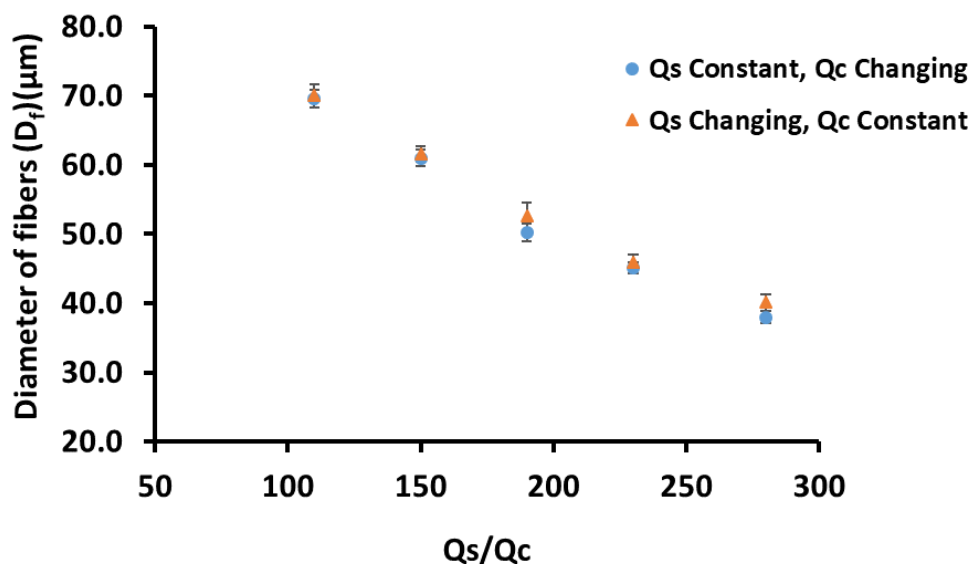


Fig. 2. Effect of Q_s/Q_c on the fiber diameter considering the effect of either the sheath flow rate (275 to 700 $\mu\text{L}/\text{min}$) at $Q_c = 2.5 \mu\text{L}/\text{min}$ (\blacktriangle) or the change core flow rate (1.07 to 2.72 $\mu\text{L}/\text{min}$) at $Q_s = 300 \mu\text{L}/\text{min}$ (\bullet) producing the same Q_s/Q_c (I.D = 50 μm , outlet tubing internal diameter = 1.06 mm, Φ_c = TPGDA/ethanol 60/40 v%, Φ_s = PEG 300).

PEG of different molecular weights (PEG 200, PEG 400) and an equivolume mixture of PEG of different molecular weight (PEG 400/PEG 600) for Φ_s were studied (**Fig. S1**). The results of diameter variation with Q_s/Q_c for all the different Φ_s are summarized in **Fig. 3**. Each curve showed the average diameter value of at least six replicates irrelevantly of the constant flow rate (Q_s or Q_c). The slopes of the curves were almost identical for each Φ_s indicating that Q_s/Q_c was a characteristic dimensionless parameter controlling the fiber diameter.

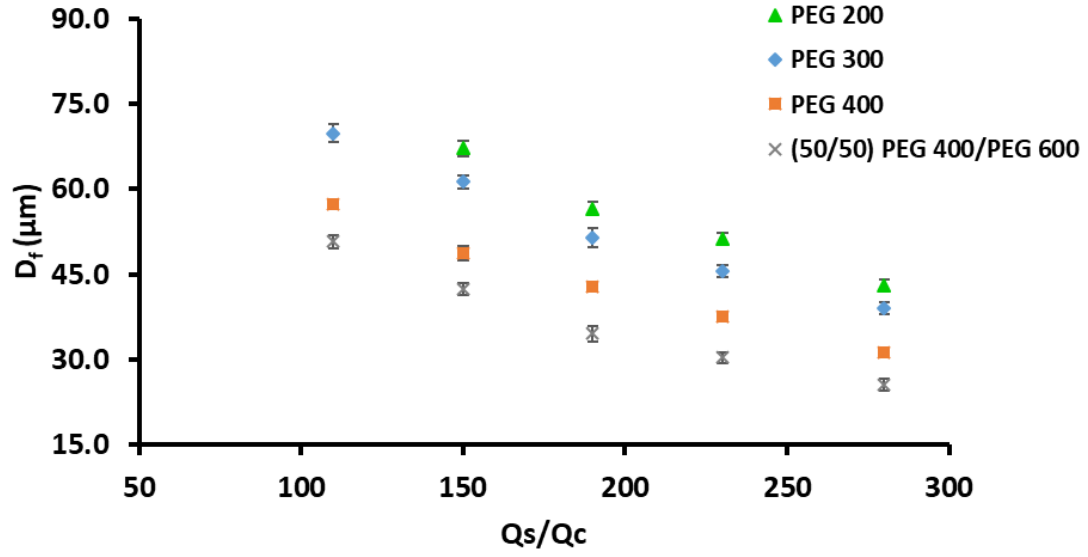


Fig. 3. Fiber diameter vs. Q_s/Q_c for different Φ_s (I.D = 50 μm , O.D = 150 μm , Φ_c = TPGDA/ethanol 60/40 v%).

2.2. Effect of viscosity ratio

The effect of viscosity ratio on the fiber diameter was investigated. While keeping the viscosity of Φ_c constant (3.14 cP) for all the experiments, the viscosity of Φ_s varied in the following order: PEG 400/PEG 600 (101.11 cP) > PEG 400 (82.11 cP) > PEG 300 (61.35 cP) > PEG 200 (42.03 cP). The fiber diameter was affected by both Q_s/Q_c and viscosity ratio (η_s/η_c) (**Fig. 4**). Higher values of Φ_s viscosity (η_s) produced fibers of lower diameter for the same Q_s/Q_c attributed to an increased shearing force induced by a more viscous Φ_s resulting into the production of thinner core jet. **Fig. 4** seemed to indicate that for a given Φ_s , the fiber diameter followed a linear decrease with the increase in η_s/η_c . Hence, η_s/η_c was also another dimensionless parameter that controlled the fiber diameter.

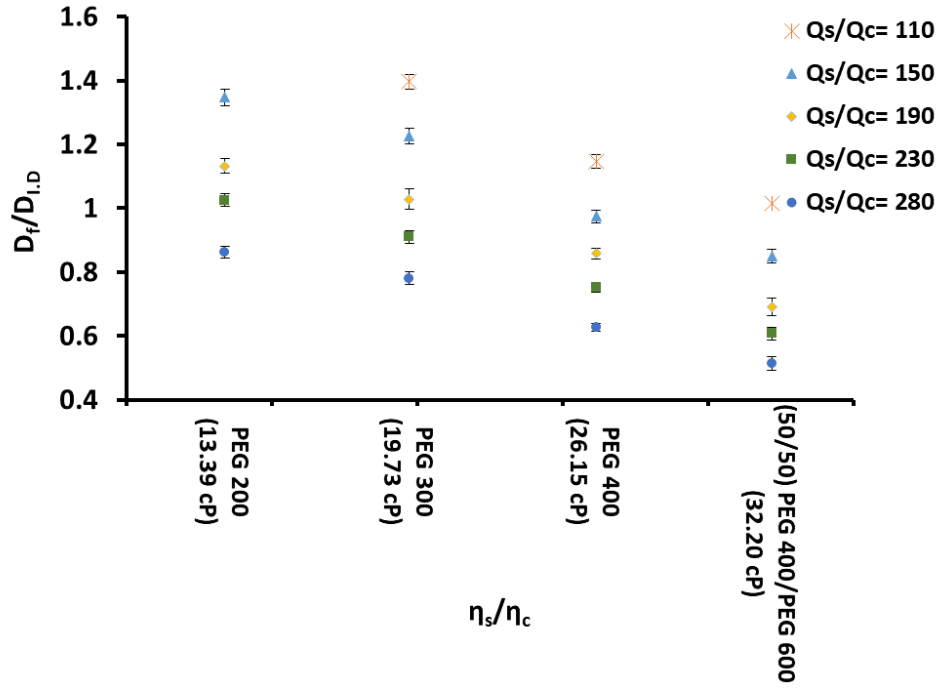


Fig. 4. Fiber diameter vs. sheath to core fluids viscosity ratio using PEG 200, PEG 300, PEG 400, PEG 400/PEG 600 as sheath fluids (I.D = 50 μ m, O.D = 150 μ m, Φ_c = TPGDA/ethanol 60/40 v%).

2.3. Capillary number ratio (Ca_s/Ca_c)

Capillary number is defined as:

$$Ca = \eta v / \gamma \quad (1)$$

where η and v are the viscosity and velocity of the fluid respectively, and γ the interfacial tension between the fluids in contact. It compares the viscous force (proportional to the shear stress) to the interfacial force (proportional to the interfacial tension) and appears as an appropriate dimensionless number to account for the effects of the fluid velocity (or flow rate) and viscosity as stressed out in the above two previous studies. Two capillary numbers can be defined, $Ca_s = \eta_s v_s / \gamma$ and $Ca_c = \eta_c v_c / \gamma$ for Φ_s and Φ_c respectively. For a given set of sheath and core fluids, the interfacial tension was the same and constant for both capillary numbers. Thus, one can define the capillary number ratio as:[38]

$$\frac{Ca_s}{Ca_c} = \frac{\eta_s \cdot v_s}{\eta_c \cdot v_c} \quad (2)$$

This ratio can simultaneously accommodate the effects of η_s/η_c and Q_s/Q_c . The latter can be expressed as a function of the velocity ratio (v_s/v_c) since the inner cross sections of the capillary and outlet tubing were kept constant for all experiments. The sheath fluid velocity (v_s) was evaluated by subtracting from the outlet tubing inner cross section the capillary outer cross section. To correlate all the data presented in the previous sections in the form of dimensionless numbers, the fiber diameter (D_f) was arbitrarily normalized by the inner capillary diameter (D_{LD}). After calculating the values of v_s/v_c from the investigated Q_s/Q_c , the capillary ratios (Ca_s/Ca_c) was accessed from **Equation 2**. The variations of the normalized fiber diameter (D_f/D_{LD}) as a function of this capillary ratio (**Fig. 5**) was plotted for all the data presented in **Fig. 4**. All data fell down to a unique master curve highlighting the decrease of D_f when the capillary number ratio was increased. The slight deviation for PEG 200 could be due to its lower viscosity allowing higher dilution of Φ_c into the bulk Φ_s . This trend complied with the separate reduction in diameter observed with an increase of Q_s/Q_c and η_s/η_c (**Fig. 3** and **4** respectively). The same trend was reported for the production of polymer microparticle and oily droplets particles.[38, 39]

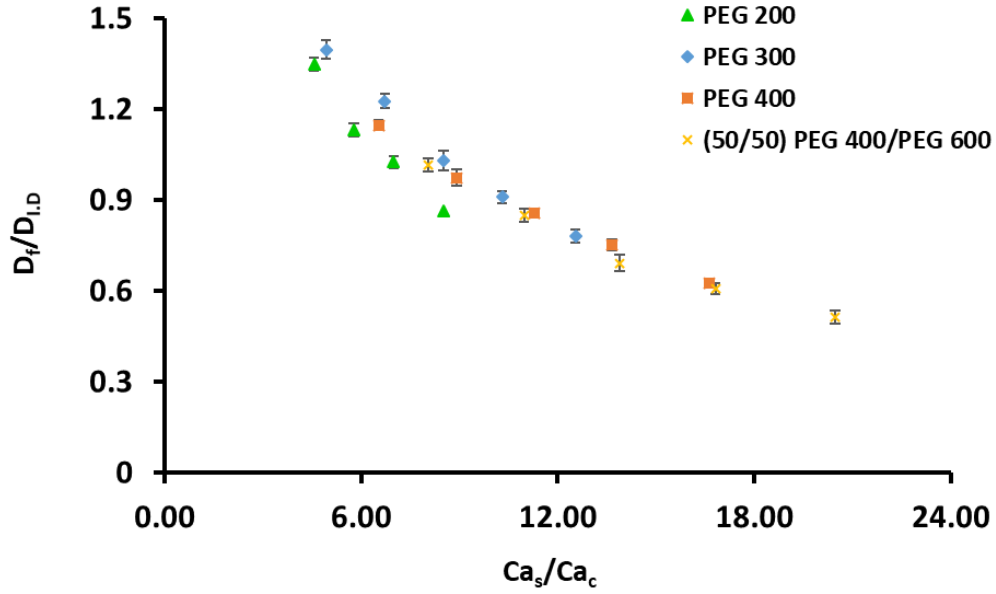


Fig. 5. Master curve presenting the variation of the diameter ratio ($D_f/D_{I,D}$) with respect to the capillary number ratio (Ca_s/Ca_c) according to the data from **Fig. 3** ($I.D = 50 \mu m$, $O.D = 150 \mu m$, $\Phi_c = \text{TPGDA/ethanol } 60/40 \text{ v\%}$).

For the determination of a useful empirical correlation between dimensionless numbers allowing the prediction of D_f as a function of operating and materials parameters, the data from **Fig. 5** were represented in a logarithm plot (**Fig. 6**) (blue curve). From the linear variation of $\ln(D_f/D_{I,D})$ with $\ln(Ca_s/Ca_c)$, the following correlation was extracted by linear regression:

$$\frac{D_f}{D_{I,D}} = K_0 \left(\frac{Ca_s}{Ca_c} \right)^{-0.63} \quad (3)$$

with $K_0 = 3.71$.

Positive values of $\ln(D_f/D_{I,D})$ in **Fig. 6** indicated fibers which diameters were greater than the inner capillary diameter while the negative values indicated smaller diameters. It was observed that a wide range of diameters, smaller or greater than the size of capillary diameter can be obtained. In the above-mentioned experiments, K_0 is a constant but could possibly vary with the capillary dimensions.

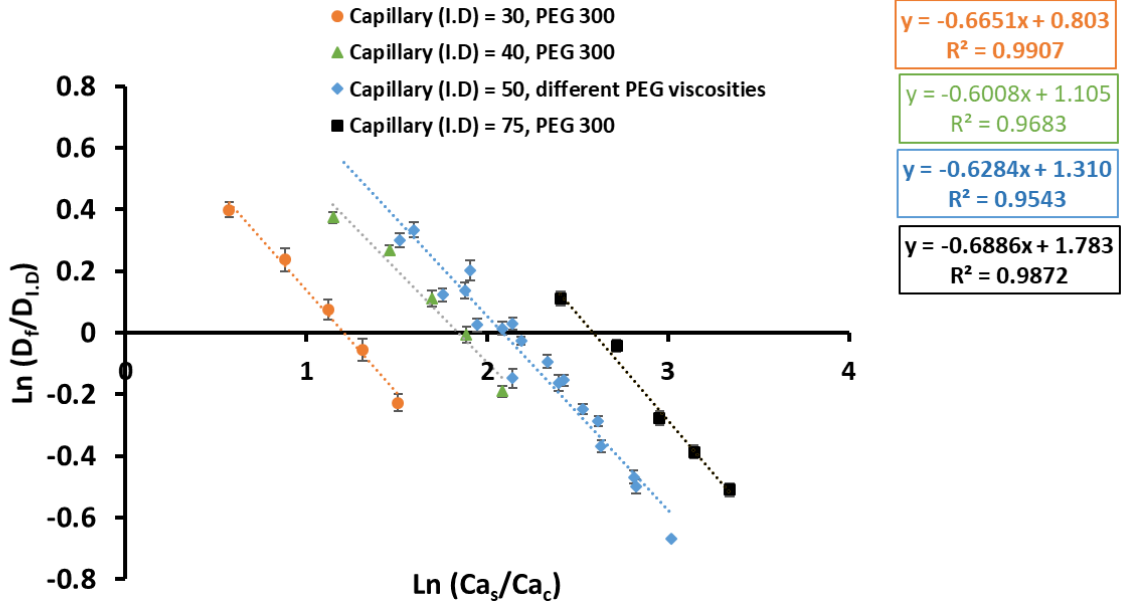


Fig. 6. Ln-Ln graph of fiber diameter variation with respect to Ca_s/Ca_c for the experimental data of **Fig. 5** (blue curve) (I.D = 30, 40, 50, and 75 μm , O.D = 150 μm). The dotted line indicates the linear regression fit (**Equation 3**).

2.4. Effect of outer and inner capillary diameter

The effect of the outer capillary diameter (O.D) on D_f was assessed using O.D of 150, 190, 280 and 365 μm , while keeping the inner diameter (I.D) equal to 50 μm ($Q_c = 2.5 \mu\text{L}/\text{min}$, while varying Q_s from 275 to 700 $\mu\text{L}/\text{min}$). The logarithm of D_f followed a linear variation with respect to the logarithm of Q_s/Q_c irrelevantly of O.D (**Fig. S2**). Furthermore, the linear regression equation was the same as the one found for the blue curve (I.D = 50 μm , **Fig. 6**). It was concluded that the capillary outer diameter did not affect D_f in the size range investigated. Inversely to the production of droplets, whose diameter is fixed when they detach from the capillary tip,[38] fiber diameter is mainly set downstream to the capillary tip when the shear stresses of Φ_s and Φ_c equilibrate. The effect of the O.D was irrelevant.

Similarly, the effect of I.D was investigated using capillaries with the same O.D (150 μm) but different I.D (30, 40, 50 and 75 μm) with the same conditions for Q_c and Q_s as the previous study

conducted with a constant I.D. Varying I.D resulted in a set of parallel lines (same slopes around -0.63) but exhibited different y-intercepts as a function of I.D (**Fig. 6**) indicating that I.D played a role on the resulting D_f through the K_0 parameter of **Equation 3**. To assess more precisely this dependence, the different y-intercepts (*i.e.* $\ln(K_0)$) values extracted from **Fig. 6** were plotted as a function of $\ln(D_{I.D})$ (**Fig. 7**) showing a linear dependence between $\ln(K_0)$ and $\ln(D_{I.D})$. This dependence can be expressed by the following equation:

$$\ln(K_0) = 1.06 \ln(D_{I.D}) - 2.82 \quad (4)$$

which can be rewritten as:

$$K_0 = \exp^{-2.82} D_{I.D}^{1.06} \quad (5)$$

Introducing K_0 into **Equation 3** and taking the average value of the slopes in **Fig. 6** (-0.65) gave:

$$\frac{D_f}{D_{I.D}} = K_1 D_{I.D}^{1.06} \left(\frac{Ca_s}{Ca_c}\right)^{-0.65} \quad (6)$$

with $K_1 = 0.06 \mu\text{m}^{-1}$.

Extracting D_f from above equation resulted in:

$$D_f = K_1 D_{I.D}^{2.06} \left(\frac{Ca_s}{Ca_c}\right)^{-0.65} \quad (7)$$

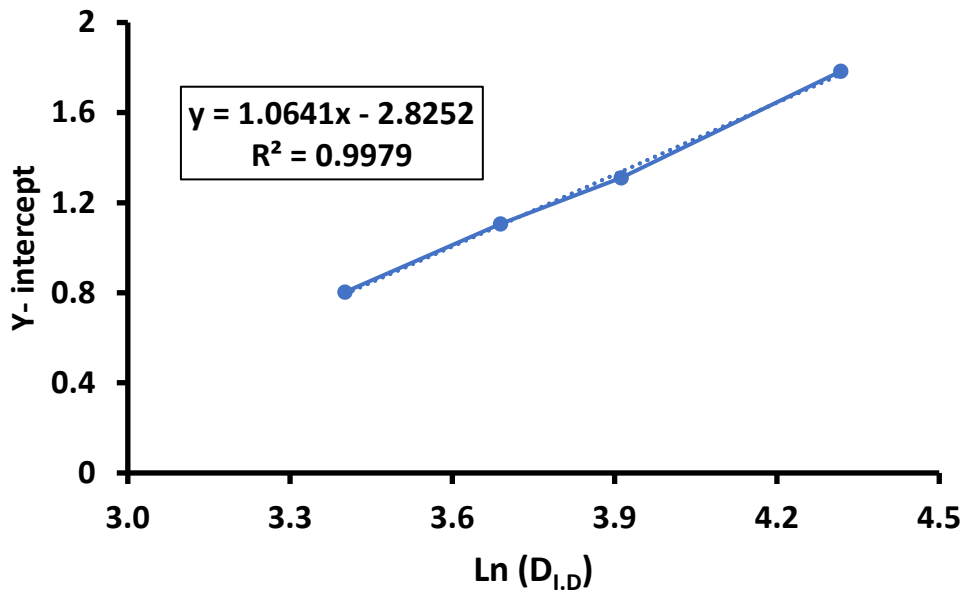


Fig. 7. Variation of the y-intercept (**Fig. 6**) with respect to logarithm of I.D (O.D = 150 μm).

2.5. Effect of monomer volume fraction

The effect of Φ_c composition was investigated by varying the monomer volume fraction ($X_{v,m}$, **Equation 8**) from 10 to 80%.

$$X_{v,m} = \frac{V_m}{V_m + V_s} \quad (8)$$

where V_m and V_s are the monomer and solvent (ethanol) volumes in core phase respectively

The logarithm of D_f followed a linear increase with respect to the logarithm of the volume fraction (**Fig. 8**) which was expressed as:

$$D_f = K_2 X_{v,m}^{0.47} \quad (9)$$

with $K_2 = 66 \mu\text{m}$.

As the monomer volume fraction increased, a larger portion of the monomer core phase volume was polymerized resulting in a thicker fiber. Experiments with $X_{v,m}$ above 80% led to clogging due to the buckling effect resulting from the fast polymerization induced by the high concentration of monomer.

By replacing K_1 (**Equation 7**) by the right-hand side expression of **Equation 9**, the overall correlation could be expressed as:

$$D_f = K_3 X_{v,m}^{0.47} D_{l,D}^{2.06} \left(\frac{Ca_s}{Ca_c}\right)^{-0.65} \quad (10)$$

K_3 was determined to be equal to $0.12 \mu\text{m}^{-1}$ by minimizing the mean squared error between all experimental D_f measured and the fiber diameters returned by **Equation 10** under same experimental conditions (**Fig. S3**). **Equation 10** represented an empirical correlation allowing a fairly well prediction of D_f , in the range of Ca_s/Ca_c between 25 and 84, as a function of operating parameters, *i.e.* I.D, individual capillary number of Φ_s and Φ_c and monomer volume fraction in Φ_c (**Fig. S3**).

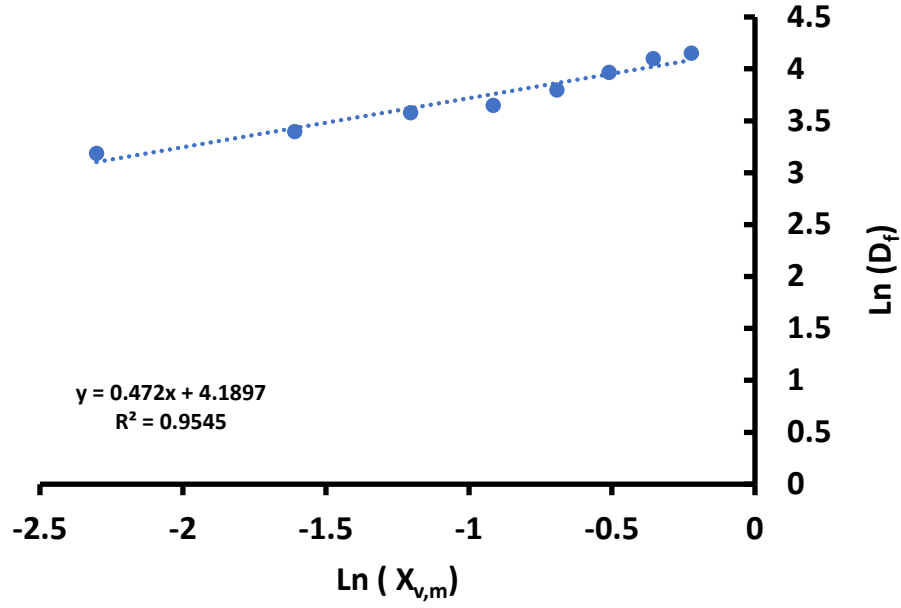


Fig. 8. Variation of the fiber diameter with respect to the monomer volume fraction (I.D = 50 μm , O.D = 150 μm , Φ_c = TPGDA/ethanol, Φ_s = PEG 300).

2.6. Effect of material system

Equation 10 was obtained with one specific material system, *i.e.* TPGDA as Φ_c and PEG as Φ_s . To check the relevancy of this empirical relationship, two additional Φ_c were investigated: PEGDA with a molecular weight of 400 g/mol and NOA 89 while keeping the same Φ_s (PEG 300). It was observed that if the slope remained the same irrelevantly of the material system studied, K_0 value (and subsequent K_3) changed noticeably (**Table 1**). The change was moderate for TPGDA and NOA 89 while it was much more pronounced for PEGDA. This must be related to the core phase viscosity (η_c , **Table 1**) which is twice higher for PEGDA than for the other two core phases investigated. Thus, one can make the hypothesis that PEGDA monomer diffuses less in the sheath phase. As a result, D_f will be thinner which will be expressed by a lower diameter and thus a lower y-intercept.

Table 1. Values of the slope, y-intercept for $\ln(D_f/D_{I.D.})$ vs. $\ln(Ca_s/Ca_c)$ plots (**Fig. S4**) and viscosity using different core phases (I.D and O.D of 50 μm and 150 μm respectively).

Core phase	Slope	y –intercept	$K_0 (\mu\text{m}^{-1})$	$\eta_s (\text{cP})$
TPGDA	-0.628	1.31	3.71	3.14
NOA 89	-0.688	1.24	3.46	3.5
PEGDA	-0.622	0.80	2.23	7.04

2.7. Monodispersity and reproducibility of fiber diameter

The robustness of the process was proved by evaluating the monodispersity and reproducibility of D_f . The coefficient of variation (CV), defined as the ratio between the standard deviation σ (**Equation 12**) of all the diameters measured and the average fiber diameter $D_{f,avg}$, was evaluated (**Fig. S5**):

$$CV = \sigma / D_{f,avg} \quad (12)$$

CV is generally reported to check against the monodispersity of micron-sized droplets or particles. It is commonly admitted that CVs below 5% are the signature of monodisperse objects. It was extended to fibers and the monodispersity was evaluated by measuring the diameter at different random locations along the fiber length for different sheath and core phase flow rates and for a capillary with I.D = 50 μm and O.D = 150 μm . It remained below 5% in all situations indicating that the developed process allowed producing monodisperse fibers (**Fig. S5a**).

As for the reproducibility, it was evaluated by determining the average diameter of fibers obtained for three batches with the same operating and material parameters carried out on different days. The results (**Fig. S5b**) indicated that whatever the sheath phase employed, the returned CVs were always lower than 5% highlighting the strong reproducibility of the process.

3. Conclusion

Polymer microfibers of two different monomers and one photocurable adhesive with diameters as low as 23 μm were produced by *in situ* photopolymerization using a capillary-based coaxial microfluidic device and a miscible PEG sheath fluid. The impact of different operating and material parameters such as volume fraction of monomer in core phase, flow rate ratio of sheath to core fluid, viscosity of the sheath fluid and dimensions of the capillary on the resulting fiber's diameter were studied. The diameter of the fiber was inversely related to the flow rate ratio and viscosity of the sheath fluid. The size of the fiber could also be varied by changing the inner diameter of the capillary but was not affected by the outer diameter. From all the data collected, an empirical relationship which precisely predicted the fiber diameter as a function of the capillary's inner diameter, monomer volume fraction and capillary number ratio of sheath to core fluid was successfully extracted. Furthermore, the coefficient of variation of the fibers' diameter was consistently less than 5% thus highlighting a robust and reproducible process for the production of monodisperse fibers.

Acknowledgments

Authors thank W. Drenckhan for discussions and A. Collard for all technical aspects. Authors are grateful to P. Allgayer for mechanical engineering support. WR would like to acknowledge the Higher Education Commission of Pakistan (HEC) for his Ph.D. fellowship.

References

- [1] X.-Y. Du, Q. Li, G. Wu, S. Chen, Multifunctional micro/nanoscale fibers based on microfluidic spinning technology, *Adv. Mater.* 31 (2019) 1903733.
- [2] M. Angelozzi, M. Miotto, L. Penolazzi, S. Mazzitelli, T. Keane, S.F. Badylak, et al., Composite ECM–alginate microfibers produced by microfluidics as scaffolds with biomineralization potential, *Mater. Sci. Eng. C* 56 (2015) 141-153.

- [3] T. Takei, N. Kishihara, S. Sakai, K. Kawakami, Novel technique to control inner and outer diameter of calcium-alginate hydrogel hollow microfibers, and immobilization of mammalian cells, *Biochem. Eng. J.* 49 (2010) 143-147.
- [4] Y.-S. Lin, K.-S. Huang, C.-H. Yang, C.-Y. Wang, Y.-S. Yang, H.-C. Hsu, et al., Microfluidic synthesis of microfibers for magnetic-responsive controlled drug release and cell culture, *PLoS One* 7 (2012) e33184.
- [5] C. Haynl, E. Hofmann, K. Pawar, S. Förster, T. Scheibel, Microfluidics-produced collagen fibers show extraordinary mechanical properties, *Nano Lett.* 16 (2016) 5917-5922.
- [6] T. Sun, Q. Huang, Q. Shi, H. Wang, C. Hu, P. Li, et al., Assembly of alginate microfibers to form a helical structure using micromanipulation with a magnetic field, *J. Micromech. Microeng.* 26 (2016) 105017.
- [7] R. Blue, D. Uttamchandani, Recent advances in optical fiber devices for microfluidics integration, *J. Biophotonics* 9 (2016) 13-25.
- [8] K. Liu, Z. Zhou, X. Yan, X. Meng, H. Tang, K. Qu, et al., Polyaniline nanofiber wrapped fabric for high performance flexible pressure sensors, *Polymers* 11 (2019) 1120.
- [9] M. Yang, J. Pan, A. Xu, L. Luo, D. Cheng, G. Cai, et al., Conductive cotton fabrics for motion sensing and heating applications, *Polymers* 10 (2018) 568.
- [10] E. Korina, O. Stoilova, N. Manolova, I. Rashkov, Polymer fibers with magnetic core decorated with titanium dioxide prospective for photocatalytic water treatment, *J. Environ. Chem. Eng.* 6 (2018) 2075-2084.
- [11] L. Jurecska, K. Barkács, É. Kiss, G. Gyulai, T. Felföldi, B. Törő, et al., Intensification of wastewater treatment with polymer fiber-based biofilm carriers, *Microchem. J.* 107 (2013) 108-114.
- [12] L. Cui, N. Zhang, W. Cui, P. Zhang, X. Chen, A Novel Nano/Micro-Fibrous Scaffold by Melt-Spinning Method for Bone Tissue Engineering, *Journal of Bionic Engineering* 12 (2015) 117-128.
- [13] O. Nechyporchuk, T. Yang Nilsson, H. Ulmefors, T. Köhnke, Wet Spinning of Chitosan Fibers: Effect of Sodium Dodecyl Sulfate Adsorption and Enhanced Dope Temperature, *ACS Applied Polymer Materials* 2 (2020) 3867-3875.

- [14] S. Liao, X. Bai, J. Song, Q. Zhang, J. Ren, Y. Zhao, et al., Draw-Spinning of Kilometer-Long and Highly Stretchable Polymer Submicrometer Fibers, *Advanced Science* 4 (2017) 1600480.
- [15] Y. Loo, S. Zhang, C.A.E. Hauser, From short peptides to nanofibers to macromolecular assemblies in biomedicine, *Biotechnology Advances* 30 (2012) 593-603.
- [16] J. Lin, B. Ding, J. Yu, Y. Hsieh, Direct Fabrication of Highly Nanoporous Polystyrene Fibers via Electrospinning, *ACS Applied Materials & Interfaces* 2 (2010) 521-528.
- [17] A. Duboin, R. Middleton, F. Malloggi, F. Monti, P. Tabeling, Cusps, spouts and microfiber synthesis with microfluidics, *Soft Matter* 9 (2013) 3041-3049.
- [18] K. Singha, S. Maity, M. Singha, P. Paul, D.P. Gon, Effects of fiber diameter distribution of nonwoven fabrics on its properties, *Int. J. Textile Sci.* 1 (2012) 7-14.
- [19] K. Young, F.M. Blighe, J.J. Vilatela, A.H. Windle, I.A. Kinloch, L. Deng, et al., Strong dependence of mechanical properties on fiber diameter for polymer-nanotube composite fibers: Differentiating defect from orientation effects, *ACS Nano* 4 (2010) 6989-6997.
- [20] H.H. Kim, M.J. Kim, S.J. Ryu, C.S. Ki, Y.H. Park, Effect of fiber diameter on surface morphology, mechanical property, and cell behavior of electrospun poly(ϵ -caprolactone) mat, *Fibers Polym.* 17 (2016) 1033-1042.
- [21] M. Chen, P.K. Patra, S.B. Warner, S. Bhowmick, Role of fiber diameter in adhesion and proliferation of NIH 3T3 fibroblast on electrospun polycaprolactone scaffolds, *Tissue Eng.* 13 (2007) 579-587.
- [22] J. Yang, F. He, H. Wu, Y. Liang, Y. Wang, Z. Sun, Engineering surface and optical properties of TiO₂-coated electrospun PVDF nanofibers via controllable self-assembly, *Nanomater.* 8 (2018) 741.
- [23] S. Chang, A.G. Fane, The effect of fibre diameter on filtration and flux distribution — relevance to submerged hollow fibre modules, *J. Membr. Sci.* 184 (2001) 221-231.
- [24] W. Jeong, J. Kim, S. Kim, S. Lee, G. Mensing, D.J. Beebe, Hydrodynamic microfabrication via "on the fly" photopolymerization of microscale fibers and tubes, *Lab Chip* 4 (2004) 576-80.
- [25] M. Hu, R. Deng, K.M. Schumacher, M. Kurisawa, H. Ye, K. Purnamawati, et al., Hydrodynamic spinning of hydrogel fibers, *Biomaterials* 31 (2010) 863-9.
- [26] A.L. Thangawng, P.B. Howell, Jr., C.M. Spillmann, J. Naciri, F.S. Ligler, UV polymerization of hydrodynamically shaped fibers, *Lab Chip* 11 (2011) 1157-60.

- [27] S. Nakajima, R. Kawano, H. Onoe, Stimuli-responsive hydrogel microfibers with controlled anisotropic shrinkage and cross-sectional geometries, *Soft Matter* 13 (2017) 3710-3719.
- [28] A.L. Thangawng, P.B. Howell, Jr., J.J. Richards, J.S. Erickson, F.S. Ligler, A simple sheath-flow microfluidic device for micro/nanomanufacturing: fabrication of hydrodynamically shaped polymer fibers, *Lab Chip* 9 (2009) 3126-30.
- [29] A. Venkateshwarlu, R.P. Bharti, Effects of capillary number and flow rates on the hydrodynamics of droplet generation in two-phase cross-flow microfluidic systems, *Journal of Taiwan Institute of Chemical Engineers* 129 (2021) 64-79.
- [30] W. Liu, Z. Xu, L. Sun, P. Guo, C. Zeng, C. Wang, et al., Polymerization-induced phase separation fabrication: A versatile microfluidic technique to prepare microfibers with various cross sectional shapes and structures, *Chemical Engineering Journal* 315 (2017) 25-34.
- [31] C.M. Hwang, A. Khademhosseini, Y. Park, K. Sun, S.-H. Lee, Microfluidic chip-based fabrication of PLGA microfiber scaffolds for tissue engineering, *Langmuir* 24 (2008) 6845-6851.
- [32] F. Wu, X.-J. Ju, X.-H. He, M.-Y. Jiang, W. Wang, Z. Liu, et al., A novel synthetic microfiber with controllable size for cell encapsulation and culture, *J. Mater. Chem. B* 4 (2016) 2455-2465.
- [33] B.K. Pullagura, V. Gundabala, Microfluidics-based on-demand generation of nonwoven and single polymer microfibers, *Langmuir* 36 (2020) 1227-1234.
- [34] M. Zhou, J. Gong, J. Ma, Continuous fabrication of near-infrared light responsive bilayer hydrogel fibers based on microfluidic spinning, *e-polym.* 19 (2019) 215-224.
- [35] Z. Bai, J.M. Mendoza Reyes, R. Montazami, N. Hashemi, On-chip development of hydrogel microfibers from round to square/ribbon shape, *M. Mater. Chem. A* 2 (2014) 4878-4884.
- [36] M. Nie, S. Takeuchi, Microfluidics based synthesis of coiled hydrogel microfibers with flexible shape and dimension control, *Sens. Actuators, B* 246 (2017) 358-362.
- [37] A. Gursoy, K. Iranshahi, K. Wei, A. Tello, E. Armagan, L.F. Boesel, et al., Facile fabrication of microfluidic chips for 3D hydrodynamic focusing and wet spinning of polymeric fibers, *Polymers* 12 (2020) 633.

- [38] C. Serra, N. Berton, M. Bouquey, L. Prat, G. Hadziioannou, A predictive approach of the influence of the operating parameters on the size of polymer particles synthesized in a simplified microfluidic system, *Langmuir* 23 (2007) 7745-7750.
- [39] E. Chiarello, L. Derzsi, M. Pierno, G. Mistura, E. Piccin, Generation of oil droplets in a non-newtonian liquid using a microfluidic T-junction, *Micromachines* 6 (2015) 1825-1835.